Palaeogeography, Palaeoclimatology, Palaeoecology 441 (2016) 890–900

Contents lists available at ScienceDirect

Palaeogeography, Palaeoclimatology, Palaeoecology

journal homepage: www.elsevier.com/locate/palaeo

Early to Middle Miocene climate in the Atacama Desert of Northern Chile

Erik Oerter [a,*], Ronald Amundson [a], Arjun Heimsath [b], Matthew Jungers [b], Guillermo Chong [c], Paul Renne [d,e]

[a] Department of Environmental Science, Policy and Management, University of California, 130 Mulford Hall, Berkeley 94720, USA
[b] School of Earth and Space Exploration, Arizona State University, Tempe, AZ, USA
[c] Universidad Católica del Norte, Antofagasta, Chile
[d] Berkeley Geochronology Center, 2455 Ridge Rd., Berkeley 94709, USA
[e] Department of Earth and Planetary Science, University of California, Berkeley 94720, USA

ARTICLE INFO

Article history:
Received 15 May 2015
Received in revised form 18 October 2015
Accepted 24 October 2015
Available online 2 November 2015

Keywords:
Paleosol
Pedogenic carbonate
Stable isotopes
Andes Mountains
Atacama paleoclimate
Hyperaridity

ABSTRACT

The Cenozoic paleoclimate of the Atacama Desert is not well known. We examined 14 early to mid-Miocene paleosols exposed in the El Tesoro Mine, near Calama, Chile. The paleosols developed on an aggrading alluvial fan system, and lie above the mineralized gravel horizons that host a copper ore body. Soil-forming conditions that oscillated between chemical weathering and clay production (humid: analogous to modern Alfisols) to environments favoring the accumulation of pedogenic carbonate (arid to semi-arid: analogous to modern Aridisols) are indicated. In contrast, the region is presently hyperarid, and soils accumulate sulfates, chlorides, and nitrates. While total chemical analyses clearly show the accumulation of Ca by the carbonate-rich paleosols, none of the soils exhibit significant losses of elements by leaching. The $\delta^{18}O$ values of the carbonates range from -8.79‰ to −3.16‰ (VPDB). The O isotope data, when combined with published data from the region, reveal a significant divergence in the O isotope composition of precipitation in the eastern and western margins of the Andean plateau since the early Miocene, suggesting that simple interpretations of declining $\delta^{18}O$ values of carbonate with increasing elevation may not be appropriate. These paleosols clearly indicate that wetter conditions prevailed in what is now the Atacama Desert during the early to mid-Miocene.

1. Introduction

The detailed climate history of the present hyperarid Atacama Desert of northern Chile is poorly known, but parts of the history can be constructed from a variety of methods. In the Mesozoic, arid conditions are interpreted to have existed based on the presence of evaporite deposits of late Triassic (Suarez and Bell, 1987; Clarke, 2006) to late Jurassic (Hartley et al., 2005) age. In the earlier segments of the Cenozoic, terrestrial cosmogenic nuclide studies of old geomorphic surfaces suggest the preservation of landforms dating from the Oligocene/Miocene boundary (Dunai et al., 2005) or Early/Middle Miocene (Evenstar et al., 2009). The lack of erosion has been interpreted to indicate relatively arid conditions since then, with interspersed pluvial episodes occurring ca. 20 Ma, ca. 14 Ma, and ca. 9 Ma (Dunai et al., 2005).

While it is probable that there is considerable variability in the spatial and temporal patterns of climate conditions in the Atacama, regional climate change during the later part of the Cenozoic is likely linked, in some manner, to the uplift history of the Andes. There is paleosol evidence of hyperarid conditions as early as 13 Ma (Rech et al., 2006). Basin sediments in the northern desert have been interpreted as suggesting a Pliocene onset of hyperaridity (Hartley and Chong, 2002), while a suite of geomorphic evidence indicates a profound aridification in the southern Atacama Desert in the late Pliocene or early Pleistocene (Amundson et al., 2012). A resolution to these seemingly conflicting estimates of the onset of hyperaridity may involve relatively high climate variability throughout the Cenozoic with multiple episodes of aridity separated by wetter intervals (Jordan et al., 2014).

A challenge for understanding the climate history of this region is identifying a long and continuous archive that may capture dynamic climate states, instead of discrete geologic units in disparate locations. Here, we present data from a buried paleosol sequence exposed in an open-pit copper mine in alluvial sediments near Calama, in northern Chile. The sediments appear to have been deposited as alluvial fans along a mountain front, and periodic abandonment of the surface by lateral fluvial migration led to local deposition hiatuses that allowed soil formation. While the geochronology is not precisely constrained, the paleosols likely formed in early to mid-Miocene times. Our observations and analyses illuminate the early Neogene paleoclimate of this region of the Atacama Desert, and suggests that it consisted of periodic oscillations between humid and semi-arid end members, probably spanning millions of years.

* Corresponding author at: Department of Geology and Geophysics, University of Utah, Salt Lake City, UT 84112, USA.
E-mail address: erikjoerter@gmail.com (E. Oerter).

http://dx.doi.org/10.1016/j.palaeo.2015.10.038
0031-0182/

2. Study location and geology

The study was located in the El Tesoro copper mine, ~60 km SSW of the town of Calama (22°57′S, 69°5′W; Fig. 1) and located along the western flank of the Cordillera de Domeyko at a surface elevation of 2290 m above sea level (masl). At this exotic-type copper deposit, gravel sediments >800 m thick strike N–S to NNE–SSW and dip NW at 10°–25° (Fig. 2) (Mora et al., 2004; Tapia et al., 2011). The gravels are divided into two main units, with the upper (Gravas II, Gravas de Caliza of Tapia et al., 2011) unconformably overlying the basal (Gravas I, Gravas de Granito of Tapia et al., 2011) (Fig. 3). Gravas I hosts the copper mineralization horizons that are interpreted to have formed by meteoric waters leaching a porphyry copper ore body and subsequent lateral advection of the mineralized fluids into gravel zones with favorable permeability. Basement faulting associated with the Domeyko fault system subsequently down dropped and isolated the mineralized gravels from any further copper enrichment (Mora et al., 2004). Gravelly sediments continued to accumulate above the mineralization, though interrupted by a depositional hiatus and erosional episode marked by the unconformity between Gravas I and Gravas II. The paleosols studied here occur in the upper part of Gravas I and throughout Gravas II (Fig. 3). The parent material for the paleosols is comprised of mixed igneous and limestone clasts with typical diameters of 1–7 cm, occasionally up to 35 cm or larger. The mode of deposition is interpreted to be high-energy stream and sheet flood events, based on the clast-supported matrix, presence of trough cross lamination sedimentary structures and sub-rounded gravel lithomorphology with gravel provenance from the east and east-southeast (Tapia et al., 2011).

The region experienced considerable uplift, tilting, and faulting since Oligocene times (Jordan et al., 2010). The heads of many Miocene fans are abruptly truncated at ~4000 m by the deep escarpment that descends into the present Salar de Atacama; while paleosol and geomorphic considerations indicate that the eastern end of the fans may have been uplifted ~900 m since the late Miocene (Rech et al., 2006), with a tilting of 1.3° to the west along the N–S monoclinal axis (Jordan et al., 2010). As a result, the present geographical setting differs substantially from that during the alluvial deposition and soil formation recorded by the paleosols.

The mean annual precipitation (MAP) of nearby Calama is 4.2 mm (Houston, 2006), and mean annual temperature (MAT) is 12 °C. Except for stream margins, the region is plant-free. Surface soils are rich in gypsum/anhydrite in the upper ~1 m, and have accumulations of chloride and nitrates at greater depths (Ewing et al., 2006). Presently, carbonate-forming environments begin at ~3200 masl (Quade et al., 2007). The surficial geology consists of expansive dissected alluvial fans of Miocene age that have inset Plio-Pleistocene surfaces. As with much of the Atacama, Quaternary landforms are largely constrained to modern stream channels and washes, and the landscape surface is dominated by Tertiary deposits.

3. Methods

3.1. Paleosol field identification and sampling

In 2010, there were two large open pits at the El Tesoro Mine, and this research was located in the southern mine. The entry road into the mine was oriented in a sub-perpendicular direction to the sedimentary dip, allowing for the observation of ~200 m of stratigraphic section (Fig. 2). The section was walked and the exposures were cleared of dust. The section contained numerous paleosols, each of which is 1 to 3 m thick, separated by many tens of meters of non-pedogenic gravelly sediments. The paleosols were easily identified by reddening, disruption of sedimentary structure, and/or distinctive secondary carbonate—all typical of modern soils. Paleosols varied greatly in degrees of development, from slightly oxidized zones (representing very short durations of exposure), to very distinctive soil profiles. Thus, only the major soils exposed in the mine were logged, described, and sampled, and the sequence ultimately chosen consisted of 14 paleosols. The sampled paleosols were well distributed along the transect and we consider them to be representative of the pedogenic variability along the entire section.

Soil profile thickness was measured from the top of the contact between uppermost horizon and overlying unaltered parent material to the approximate base of pedogenic alteration. Each soil was morphologically described *in situ* (Soil Survey Staff, 1999). The paleosols were sampled by horizon for bulk soil material and carbonate-bearing clasts for geochemical and carbonate stable C and O isotope analyses. All paleosols were lithified to varying degrees, and sample collection usually involved a hammer and chisel. Samples of the overlying non-pedogenic gravel were also collected to represent unweathered parent material or to compare to the weathered material below. Detailed stratigraphic measurement of the non-pedogenic gravels and the gravel package as a whole was not possible due to access and time limitations in the actively producing mine at El Tesoro.

3.2. Laboratory methods

Bulk samples were disaggregated by light crushing in a mortar and pestle or by jaw crusher and then passed through a 2 mm sieve to separate the fine fraction. Munsell soil color value determinations were made on the dry <2 mm fine fractions. Sub-samples of approximately 150 g were taken from the <2 mm fraction to be analyzed for major

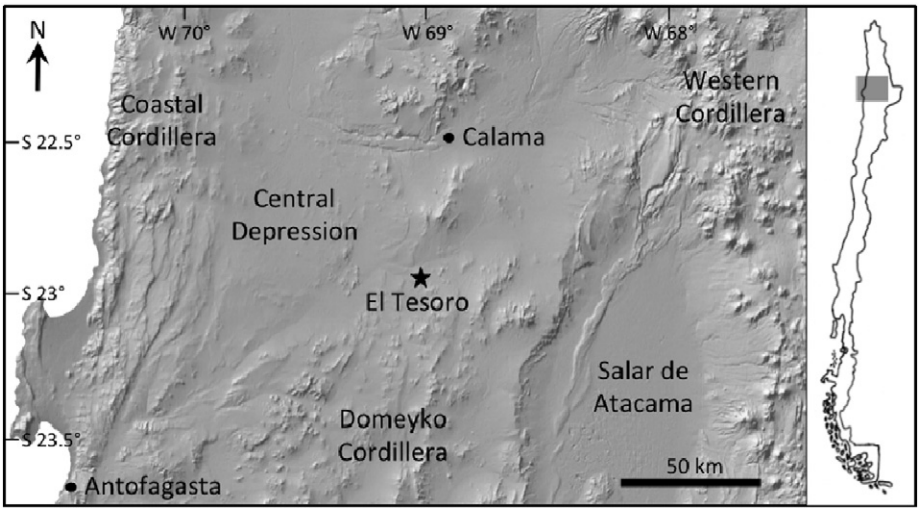

Fig. 1. Map of northern Chile with the El Tesoro mine location marked with star and nearby physiographic features.

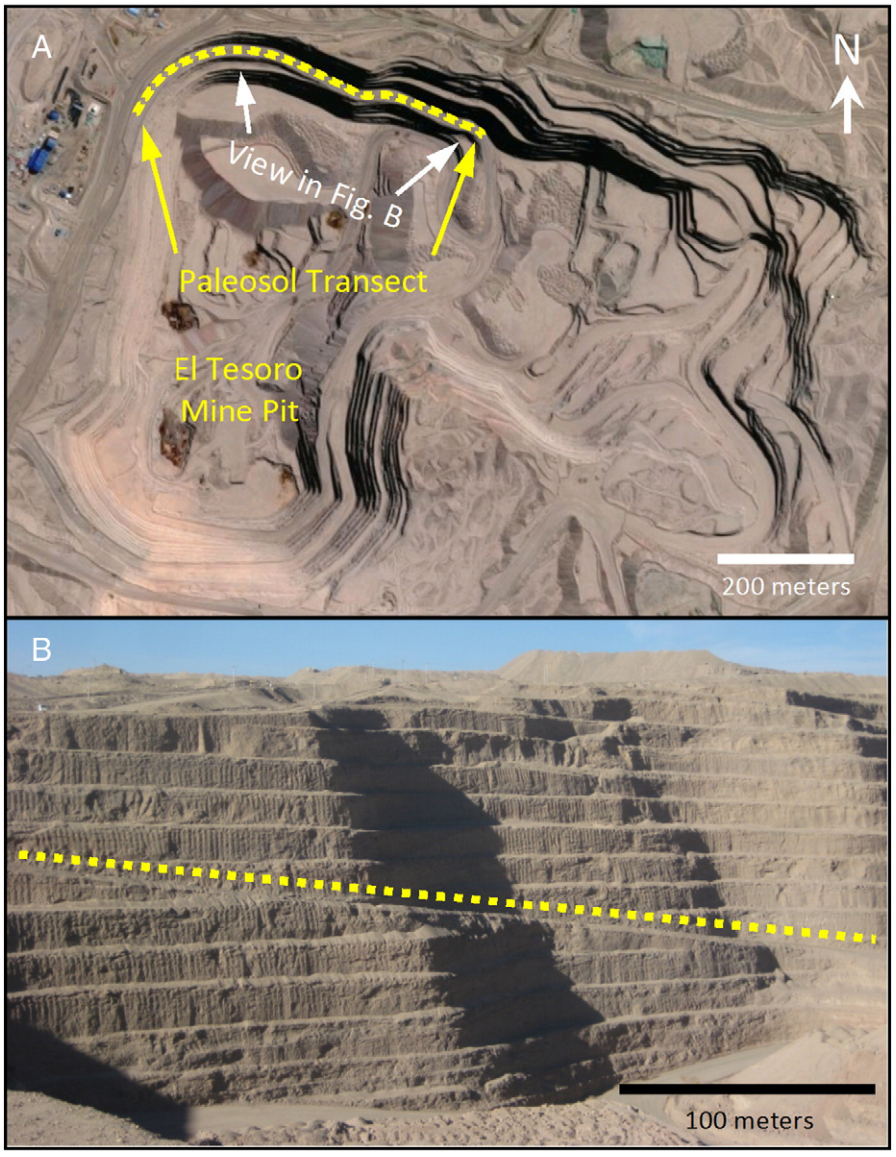

Fig. 2. (A) Aerial view of El Tesoro mine pit showing location of paleosol transect (yellow dashed line) (image: Google); (B) photograph of mine pit wall in area of paleosol transect, the mine road along which the sampling was done is the prominent sub-horizontal plane (yellow dashed line) descending from left to right in photo (image: Compania Minera El Tesoro).

elements and principal metals by inductively coupled plasma atomic emission spectra, carbon and sulfur by Leco induction furnace, and trace elements by inductively coupled plasma mass spectrometry at ALS-Chemex Laboratories in Reno, NV.

The presence of carbonate in the <2 mm fine fraction was determined by reaction with dilute HCl, and small (~5 g) sub-samples of carbonate-bearing fine material were taken for carbonate abundance (weight %), $\delta^{13}C$ and $\delta^{18}O$ values. Carbonate coating material from several clasts in each horizon was removed by scraping, combined and lightly ground by hand with a mortar and pestle. All carbonate samples (fines and clast coating material) were washed with a distilled water rinse through filter paper to remove salts accumulated during atmospheric exposure in the mine pit and oven dried at 70 °C overnight. Measurement of carbonate $\delta^{13}C$ and $\delta^{18}O$ values were made on a dual inlet GV Isoprime gas source isotope ratio mass spectrometer with MultiCarb sample introduction interface at UC Berkeley.

Isotope values are reported in δ notation: $\delta = (R_{sample}/R_{standard} - 1) \times 1000$,

where R_{sample} and $R_{standard}$ are the $^{13}C/^{12}C$ or $^{18}O/^{16}O$ ratios for the sample and standard, respectively. Carbonate $\delta^{13}C$ and $\delta^{18}O$ values are reported in per mille (‰) referenced to the Vienna Pee Dee Belemnite (VPDB) standard, and $\delta^{18}O$ values of H_2O are reported in per mille (‰) referenced to Vienna Standard Mean Ocean Water (VSMOW) (Coplen, 1994).

4. Chronostratigraphic background and ignimbrite dating results

The age of the sediments in which the paleosols are found broadly constrain the time interval represented by the paleosols because each paleosol formed subsequent to periodic cessation of sediment deposition. The maximum age of the entire sediment sequence in the mine (Gravas I and II; Fig. 3) is constrained by underlying intrusive rocks in the Quebrada Mala Formation at 37 Ma (Mora et al., 2004). Supergene Cu mineralization formed in gravels above the Quebrada Mala but below the paleosols is dated to 21.9 Ma by K-Ar on cryptomelane (Fig. 3) (Sernageomin, 2011). Additional supergene Cu mineralization ages have been determined to be 19.2–22.9 Ma in the nearby ore deposits of Telegrafo and Polo Sur by $^{40}Ar/^{39}Ar$ dating on alunite (Tapia et al., 2011).

Supergene mineralization requires sufficient meteoric water to proceed and therefore these dates indicate the time that the mineralized sediments were near the land surface and exposed to vadose water and ground water in a wetter climate (Alpers and Brimhall, 1988). The genetic

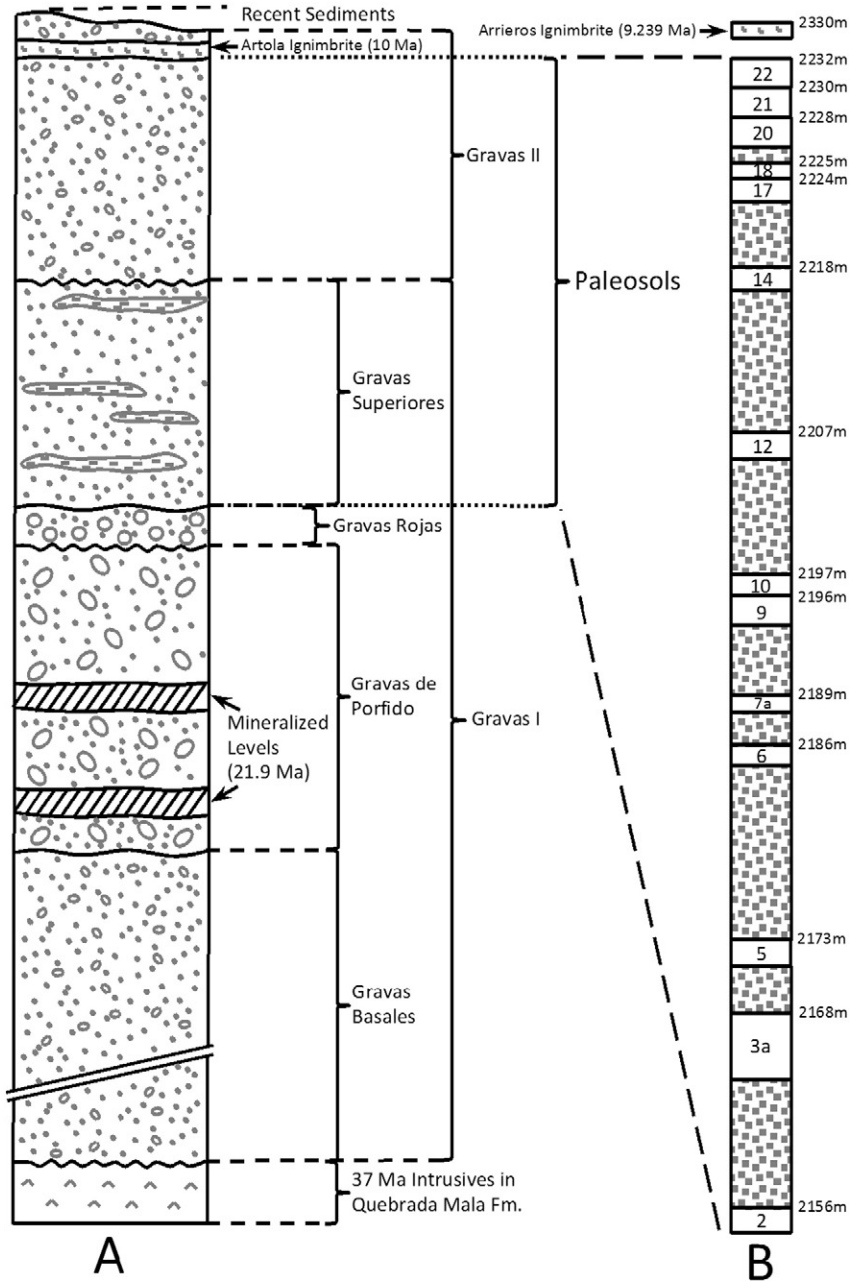

Fig. 3. (A) Stratigraphic relationship of sedimentary gravel units to dated bedrock and ignimbrite at El Tesoro (redrawn from Mora et al., 2004); (B) stratigraphic arrangement and top elevations of paleosols at El Tesoro (numbered, elevations are surveyed and uncorrected for sedimentary dip direction and magnitude), and ignimbrite from Quebrada de los Arrieros.

model for ore formation at El Tesoro indicates that the exotic copper mineralization ceased as the primary copper ore body source was depleted (Mora et al., 2004). Subsequent reverse faulting created additional sediment deposition above the mineralization, and the paleosols formed sequentially as the alluvial fans periodically alternated between periods of aggradation followed by surface stabilization. Thus, the maximum age of the paleosols is the 21.9 Ma age of mineralization.

While no directly dateable materials were found in the paleosol sequence, the minimum age of the paleosols is established by outcrops in the mine of Artola ignimbrite that have been dated at 10 Ma, by $^{40}Ar/^{39}Ar$ on biotite (Mora et al., 2004; Tapia et al., 2011), and is intercalated with the upper levels of the Gravas II unit immediately above the paleosol sequence (Fig. 3). Further validation of this minimum age is provided by results from an ash embedded in regional surficial alluvial deposits exposed in a stream cut of the Quebrada de los Arrieros approximately 8 km northeast of the paleosols that was identified and sampled during this study (−22°53′34.659″, −69°1′12.896″, 2330 masl). Individual laser fusion analyses of ten crystals of sanidine (see Supplementary Fig. 1 and Supplementary Table 1) yielded a unimodal age distribution with a weighted mean $^{40}Ar/^{39}Ar$ age of 9.239 ± 0.110 Ma based on the calibration of Renne et al. (2011). The similarity in ages between the Arrieros ignimbrite and the Artola ignimbrite, which has been dated to 9.4 Ma elsewhere in the region (De Silva, 1989), suggests that the Arrieros ignimbrite is equivalent to the Artola ignimbrite outcrops in the mine overlying the El Tesoro paleosols.

5. Results and interpretation

5.1. Paleosol morphology

The stratigraphic arrangement and pedologic characteristics of the paleosols are shown in Fig. 3 and Table 1. The paleosols are situated

Table 1
Summary of field descriptions and pedogenic carbonate abundance, accumulation times, and $\delta^{13}C$ and $\delta^{18}O$ values.

					Carbonate in <2 mm fines						Carbonate coatings	
					Wt. %	$\delta^{13}C$	$\delta^{18}O$	$CaCO_3$	Total $CaCO_3$	$CaCO_3$	$\delta^{13}C$	$\delta^{18}O$
Paleosol	Depth (cm)	Horizon	Munsell Color	Color	$CaCO_3$	(VPDB)	(VPDB)	(kg m^{-2})	(kg m^{-2})	Accumulation (year)	(VPDB)	(VPDB)
22	0–8	A	5YR 5/8	Yellowish red	–	–	–	–	–	–	–	–
	8–29	Bt	2.5YR 4/8	Red	–	–	–	–	–	–	–	–
	29–44	Bkm	7.5YR 6/4	Light brown	27.08	−3.14	−4.31	65.00			−2.32	−3.54
	44–62	Bk1	5YR 6/4	Light reddish brown	33.92	−2.67	−3.72	97.69			−2.08	−3.24
	62–78	Bk2	5YR 5/6	Yellowish red	18.07	−2.80	−3.65	46.27			−2.53	−3.16
	78–90	Ab	5YR 6/4	Light reddish brown	26.66	−2.54	−3.60	51.19			−2.51	−3.78
	90–108	Bkmb1	5YR 5/8	Yellowish red	3.02	−3.03	−3.82	8.70			−2.98	−3.77
	108–124	Bkmb2	5YR 6/4	Light reddish brown	24.69	−2.80	−3.80	63.21			−2.75	−3.60
	124–152	Bkmb3	7.5YR 6/4	Light brown	27.48	−2.75	−3.56	123.11			−2.48	−3.70
	152–190	Bkmb4	7.5YR 6/4	Light brown	24.32	−2.68	−3.46	147.86	603.02	1998279	−2.71	−3.76
21	0–32	AB	7.5YR 5/4	Brown	1.10	−3.49	−5.83	5.61	5.61	18597	–	–
	32–56	Bty	5YR 4/6	Yellowish red	–	–	–	–	–	–	–	–
	56–95	Bt1	5YR 4/4	Reddish brown	–	–	–	–	–	–	–	–
	95–135	Bt2	5YR 6/4	Light reddish brown	–	–	–	–	–	–	–	–
	135–180	BC or C	7.5YR 6/4	Light brown	–	–	–	–	–	–	–	–
20	0–28	A	5YR 4/6	Yellowish red	–	–	–	–	–	–	–	–
	28–47	Bt1	5YR 5/6	Yellowish red	5.43	−3.89	−5.30	16.51			−3.84	−4.97
	47–70	Bt2	5YR 5/8	Yellowish red	5.46	−3.38	−4.90	20.08			−3.04	−4.15
	70–99	Btk	7.5YR 6/4	Light brown	18.81	−3.29	−4.71	87.29			−3.50	−4.67
	99–114	Bk1	7.5YR 6/4	Light brown	19.13	−3.64	−4.98	45.92			−3.60	−5.03
	114–137	Bk2	7.5YR 6/4	Light brown	11.25	−3.74	−4.73	41.38			−3.38	−4.67
	137–174	Bk3	7.5YR 6/4	Light brown	6.40	−3.52	−4.51	37.90			−3.45	−4.72
	174–194	Bk4	10YR 6/3	Pale brown	24.38	−2.97	−4.47	78.00	327.08	1083875	−2.79	−4.29
18	0–8	Bk1	10YR 6/3	Pale brown	1.86	−4.11	−7.06	2.38			–	–
	8–31	Bkm	10YR 6/4	Light yellowish brown	3.71	−4.03	−6.69	13.66			−3.53	−5.16
	31–47	Bk'	10YR 6/4	Light yellowish brown	–	–	–	–	16.03	53134	−4.84	−8.79
17	0–7	A	5YR 5/6	Yellowish red	–	–	–	–	–	–	–	–
	7–20	Bt/Bw	5YR 5/8	Yellowish red	1.89	−3.81	−6.19	3.94			−3.56	−5.48
	20–43	Bk1	7.5YR 6/4	Light brown	5.07	−3.76	−5.68	18.65			−3.50	−5.44
	43–71	Bk2	7.5YR 5/4	Brown	4.49	−3.84	−5.66	20.13			−3.36	−5.33
	71–99	Bk3	7.5YR 6/4	Light brown	3.95	−3.43	−5.68	17.68			−3.12	−5.23
	99–122	Bk4	7.5YR 6/4	Light brown	3.58	−3.21	−5.55	13.18			−2.93	−5.50
	122–151	Bk5	5YR 5/8	Yellowish red	2.29	−3.83	−5.44	10.63	84.21	279039	−3.71	−4.90
14	0–14	A	7.5YR 5/4	Brown	4.35	−2.34	−6.32	9.73			−2.82	−6.40
	14–51	Bk1	7.5YR 5/4	Brown	4.16	−2.56	−6.40	24.60			−2.66	−6.57
	51–78	Bk2	7.5YR 5/3	Brown	3.70	−2.38	−6.34	15.99			–	–
	78–104	Bk3	7.5YR 5/4	Brown	0.62	−3.08	−6.51	2.60			−2.92	−6.13
	104–137	Bk4	7.5YR 6/4	Light brown	3.15	−2.70	−7.05	16.63			−2.65	−6.54
	137–155	Bk5	7.5YR 5/3	Brown	2.24	−3.35	−6.52	6.44	76.00	251836	−3.55	−6.46
12	0–23	A	5YR 5/6	Yellowish red	–	–	–	–	–	–	–	–
	23–65	Bt1	5YR 5/4	Reddish brown	–	–	–	–	–	–	–	–
	65–110	BC	5YR 5/6	Yellowish red	–	–	–	–	–	–	–	–
	110–121	C1	7.5YR 6/4	Light brown	2.79	−2.39	−6.73	–	4.90	16238	−2.41	−6.35
	121–152	C2	10YR 5/6	Yellowish brown	–	–	–	–	–	–	–	–
	152–182	C3	10YR 5/8	Yellowish brown	–	–	–	–	–	–	–	–
10	0–12	A	5YR 4/6	Yellowish red	–	–	–	–	–	–	–	–
	12–61	Bt	5YR 4/6	Yellowish red	–	–	–	–	–	–	−3.50	−5.36
	61–80	Btk	5YR 5/4	Reddish brown	18.73	−3.95	−4.35	56.95			−4.08	−4.42
	80–110	Bk1	5YR 5/4	Reddish brown	4.23	−3.54	−5.03	20.33			−2.28	−5.05
	110–136	Bk2	5YR 5/4	Reddish brown	–	–	–	–			–	–
	136–161	Bk3	5YR 5/4	Reddish brown	1.78	−4.12	−6.01	7.13	84.41	279717	−1.99	−5.41
	161–174	Bk4	5YR 5/4	Reddish brown	–	–	–	–	–	–	–	–
9	0–29	Bt1	5YR 4/6	Yellowish red	–	–	–	–	–	–	–	–
	29–83	Bt2	5YR 4/6	Yellowish red	–	–	–	–	–	–	–	–
	83–138	Btb1	5YR 4/6	Yellowish red	–	–	–	–	–	–	–	–
	138–173	Btb2	2.5YR 4/6	Red	–	–	–	–	–	–	–	–
	173–201	Btb3	5YR 4/6	Yellowish red	–	–	–	–	–	–	–	–
7a	0–10	A	10YR 6/4	Light yellowish brown	2.37	−3.01	−8.26	3.79			−2.34	−7.65
	10–28	Bk1	10YR 5/8	Yellowish brown	2.61	−1.91	−7.06	7.51			−1.42	−6.84
	28–40	Bk2	10YR 6/4	Light yellowish brown	3.78	0.14	−5.61	7.25			0.19	−5.16
	40–60	Bk3	10YR 6/6	Brownish yellow	4.21	−1.51	−5.96	13.48			−3.03	−4.55
	60–73	Bk4	10YR 5/6	Yellowish brown	2.89	−1.28	−7.86	6.01	38.04	126047	0.93	−5.38
6	0–8	Bt1	5YR 4/6	Yellowish red	–	–	–	–	–	–	–	–
	8–36	Bt2	5YR 4/6	Yellowish red	–	–	–	–	–	–	–	–
	36–49	BC	5YR 4/6	Yellowish red	–	–	–	–	–	–	–	–
	49–92	C1	7.5YR 5/6	Strong brown	–	–	–	–	–	–	–	–
	92–122	C2	10YR 5/6	Yellowish brown	–	–	–	–	–	–	–	–
5	0–15	A	5YR 5/8	Yellowish red	–	–	–	–	–	–	–	–
	15–37	Bk1	5YR 5/6	Yellowish red	4.19	2.62	−6.34	14.74			2.55	−6.13
	37–58	Bk2	5YR 5/6	Yellowish red	6.00	2.46	−6.14	20.17			2.47	−6.23
	58–73	Ab	5YR 5/6	Yellowish red	–	–	–	–			–	–

Table 1 (*continued*)

					Carbonate in <2 mm fines						Carbonate coatings	
					Wt. %	$\delta^{13}C$	$\delta^{18}O$	$CaCO_3$	Total $CaCO_3$	$CaCO_3$	$\delta^{13}C$	$\delta^{18}O$
Paleosol	Depth (cm)	Horizon	Munsell Color	Color	$CaCO_3$	(VPDB)	(VPDB)	(kg m^{-2})	(kg m^{-2})	Accumulation (year)	(VPDB)	(VPDB)
	73–98	Bk1	5YR 5/6	Yellowish red	3.37	2.16	−6.73	12.40			2.21	−6.67
	98–141	Bk2	5YR 5/6	Yellowish red	1.86	1.72	−6.19	12.82			2.10	−6.04
	141–183	Bk3	5YR 5/4	Reddish brown	3.43	1.78	−6.27	23.03	83.15	275553	2.70	−6.42
3a	0–13	Bw1	–	–	–	–	–	–	–	–	–	–
	13–40	Bw2	–	–	–	–	–	–	–	–	–	–
	40–93	Bw3	5YR 6/4	Light reddish brown	2.54	−0.52	−7.17	21.55			−0.07	−7.31
	93–313	Bkm	7.5YR 7/2	Pinkish gray	42.82	−5.20	−4.21	1507.20			−5.47	−4.13
	313–336	Bk1	7.5YR 6/3	Light brown	2.36	0.37	−7.29	8.69			0.57	−7.01
	336–356	Bk2	7.5YR 6/3	Light brown	5.21	0.42	−6.89	16.66			0.39	−7.25
	356–416	Bk3	7.5YR 6/4	Light brown	4.24	−1.34	−6.88	40.74	1594.85	5284983	0.10	−7.02
2	15–40	Bt1	7.5YR 5/4	Brown	–	–	–	–	–	–	–	–
	40–55	2Bkm1	7.5YR 7/3	Pink	36.51	−4.74	−4.38	87.62			−5.38	−4.52
	55–95	2Bkm2	7.5YR 6/4	Light brown	13.77	−4.11	−5.35	88.10			−4.61	−4.22
	95–110	Bk	7.5YR 6/2	Pinkish gray	12.58	−0.34	−6.46	30.19			−0.10	−7.08
	110–125	Bkm1′	7.5YR 6/1	Gray	42.66	−5.19	−4.39	102.38			−4.40	−4.83
	125–175	Bkm2′	7.5YR 7/1	Light gray	45.00	−5.31	−4.17	359.99	668.29	2214563	−5.40	−4.49

either directly on top of each other or are stratigraphically separated by up to several meters of non-pedogenic gravels accumulated during regional aggradation (Fig. 3). Some of the paleosols were clearly truncated by subsequent erosion before burial and appear to be missing at least portions of the A (surface) horizons. Only one soil had clear evidence of biological processes: a small animal or root burrow. The paleosols are extremely well preserved due to minimal overburden pressures and little aqueous diagenesis evidenced by undistorted pedogenic horizons as well as the preservation of some undistorted primary depositional sedimentary features found in a Fluvent-type paleosol (paleosol 7a, Table 1).

Paleosols 6, 9, 12, and 21 have strong profile and horizon development. Each had sandy soil horizons that overlie well-developed Bt horizons consisting of a dense, clay-rich matrix that in some soils formed distinctive blocky structure that surrounded gravel parent material clasts (Fig. 4A). These accumulations of clay minerals indicate the presence of enough soil water with long enough residence times to weather primary minerals and translocate the secondary clays. Paleosols 6, 9, 12, and 21 are similar to modern Alfisols (Argillisols in the Mack system), which often display argillic horizons and form in soils of temperate and humid to subhumid climates.

Paleosols 2, 3a, 10, 14, 20, and 22 showed a low degree of pedogenesis in terms of horizon development and soil structure but showed enough soil formation to disrupt the original parent material alluvial depositional stratification. They had sandy surface horizons that were partly truncated, with underlying weakly developed Bt horizons (Fig. 4B). The Bt horizons show evidence of downward translocation of clays with some clay films (argillans) present on gravels and some showed evidence of clay swelling or expansion associated with hydration. Bk horizons were always found in the depth profile and contained accumulations of pedogenic carbonate varying in their degree of development from coatings and rinds on gravel clasts, to moderate cementation of the fine matrix, to massive accumulations >1 m thick. Paleosols #5 and 18 lacked clay-bearing horizons and associated evidence of downward translocation of clays, but relatively strong calcareous horizon development. Paleosol 17 had an incipient Bt/Bw horizon (evidence of weathering and clay formation) overlying a series of calcareous Bk horizons.

These Aridic paleosols clearly formed in a carbonate-accumulating environment. Modern climates that produce Aridisols are found where evapotranspiration is greater than precipitation, typically in regions with <60 cm MAP (Schaetzel and Anderson, 2005). However, the lower limit to pedogenic carbonate forming conditions is found in hyperarid climates with <20 mm MAP and an absence of biological CO_2 (Ewing et al., 2006; Quade et al., 2007). Except for paleosols 5 and 18, these Aridic paleosols are analogous to modern Calciargids (Aridisol soil order; Argillic Calcisols in the Mack et al. (1993) paleosol classification). In general, modern Calciargids are usually soils that have undergone a climate change from a clay-forming environment (subhumid) to a subsequent carbonate-forming environment (arid).

Paleosol 7a was weakly developed and consisted of layers of fine to coarse sand and cobble sediments that are interpreted to have been deposited in lower energy portions of the fluvial systems active on the alluvial fan surface. Pedogenesis in this paleosol is very weak with the original depositional texture and structure unmodified by pedogenesis. This paleosol had a calcareous Bk horizon, and this paleosol shows carbonate accumulation indicative of climate conditions with not enough precipitation to strip carbonate out of the soil profile.

This qualitative field evidence is remarkable in that these paleosols represent unambiguous evidence of oscillating soil-forming conditions between humid environments that produce Alfisols via chemical weathering and authigenic clay production and no carbonate accumulation (humid-type), to arid and semi-arid climates that facilitate the accumulation of pedogenic carbonate typical of Aridisols (arid-type).

5.2. Paleosol geochemistry

Field observations of the El Tesoro paleosols suggest that some of the soils have undergone a considerable period of chemical weathering and authigenic clay development, while others show evidence for accumulation of pedogenic carbonate formation and accumulation. These observations should be reflected in geochemical gain and loss analyses of paleosols, and can augment the interpretation of morphological features. We used mass balance calculations relative to an immobile index element to examine gains and losses of chemical elements in each paleosol horizon relative to parent material in order to elucidate both the production of weathering products and their redistribution in the soil profile (Brimhall and Dietrich, 1987). A limitation of this technique in fluvial settings is the large heterogeneity of the lithological/mineralogical composition of the parent material sediment with space and time.

In this approach, the selection of an appropriate index element that is both homogeneously distributed throughout the soil profile and remains immobile during weathering is a primary consideration. The El Tesoro paleosol parent material was deposited in an alluvial fan setting, and will reflect the integrated chemical and mineralogical composition

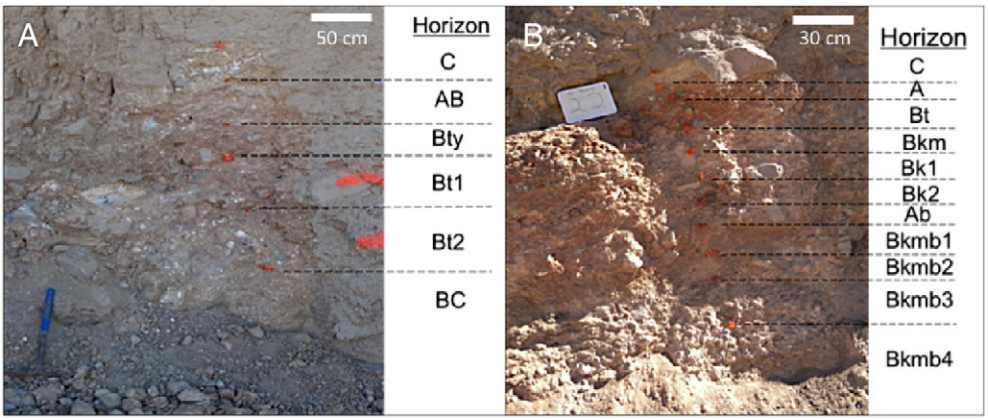

Fig. 4. (A) Photograph of paleosol analogous to a modern Alfisol (paleosol 21), note cobbles in clay-rich matrix; (B) photograph of paleosol analogous to a modern Aridisol (paleosol 22), this is a compound paleosol with the boundary between the upper and lower paleosols at the Bk2-Ab interface. See Supplemental Fig. 1 for photographs of all paleosols.

of the sediment source areas upstream. However, as this sediment is progressively transported downstream (evidenced by the rounded geometry of the parent material gravels and cobbles) physical processes result in the sorting of sediments by size and density. The resulting stochastic nature of the sediment in any stratigraphic layer creates difficulty in selecting an index element that is not affected by transport and sorting. Titanium and zirconium are often chosen as immobile index elements for mass balance analyses, but are not ideal for fluvial parent material sediment because they tend to be concentrated in heavy and more rare accessory minerals (sphene specific gravity ≈ 3.6 and zircon ≈ 4.5, compared to quartz and feldspar ≈ 2.6), especially in igneous plutonic rocks such as those from which the parent material at El Tesoro is derived.

In contrast, rare earth elements (REE) and their neighbors on the periodic table present several advantages as index elements because they are relatively well distributed in igneous silicate rocks, albeit at fairly low concentrations. Cerium, neodymium and thorium (not typically considered a REE) are relatively abundant in minerals of the continental crust, and show coherent behavior in most sedimentary processes and may thus be less subject to variations in source or physical sorting (Gromet and Silver, 1983). Pairs of elements that are both homogeneously distributed and immobile will show constant ratios throughout a soil profile (Kurtz et al., 2000). In the El Tesoro paleosols, Ce concentrations are well correlated with Nd or Th (Supplementary Data). While Ce is found in certain environments to respond to redox reactions, the generally mild weathering conditions suggested by the soils, its coherence with Nd and Th, and its relatively high abundance appear to make it suitable as an index element. Thus we used Ce as the index element to examine pedogenesis and the extent of weathering within each paleosol.

Geochemical mass balance analyses reveals two features. First, (as expected) aridic soils have large gains of Ca relative to those interpreted to be more humid (Fig. 5). Second, analysis of major element trends (Si, Fe, Na, etc.) reveals no distinctive total or depth differences between the carbonate and non-carbonate soils, indicating that the extent of chemical alteration that the soils experienced was at best modest, and was not large enough to overprint the inherent chemical variability in the sediment (Supplementary Fig. 2 and Supplementary Table 2). Additionally, many of the elements mobilized by weathering may have been retained in secondary phyllosilicates and oxides. This observation is likely reflective of both the duration of weathering, and the environmental conditions that impacted the rates of the soil-forming conditions at that time.

5.3. Paleosol carbonate occurrence and abundance

The carbonate in the El Tesoro paleosols is present in a wide variety of forms. Fine matrix carbonate is found in the B horizons of all of the aridic soils (Table 1). Carbonate coatings on gravel clasts were also common on the bottoms of clasts, a pedogenic feature reliably found in soils in modern semi-arid to arid regions, where carbonate is moved downward with migrating waters, accumulating were evapotranspiration drives calcite supersaturation (Gile et al., 1966; Amundson et al., 1997). Carbonates are also found in clay bearing Bt horizons in some paleosols at El Tesoro. The older and lower calcareous paleosols (2, 3a, 5, 7a) have much higher carbonate contents and some petrocalcic horizons are present in these lowest paleosols (Table 1).

An important determination must be made between carbonate formed *in situ* in the soil during pedogenesis (pedogenic carbonate) and that originating from carbonate-bearing parent material or from carbonate brought into the soil after development, possibly leached from above and down into the soil or added from below by fluctuating groundwater levels. Carbonate found in a soil or paleosol profile as coatings or rinds on gravel clasts is undoubtedly pedogenic, especially if it is found systematically on either the clast bottoms (commonly) or tops (less common) (Amundson et al., 1997). Clast coatings with a variety of orientations or that show evidence of abrasion due to gravel transport are doubtfully pedogenic. At El Tesoro, carbonate clast coatings are found on the bottoms of in-place soil clasts across the range of sampled paleosols and are therefore considered pedogenic in origin. The pedogenic origin of carbonate found in the <2 mm fine paleosol matrix can be confirmed by comparing its stable isotopic composition to that of carbonate clast coatings co-occurring in the same paleosol horizon,

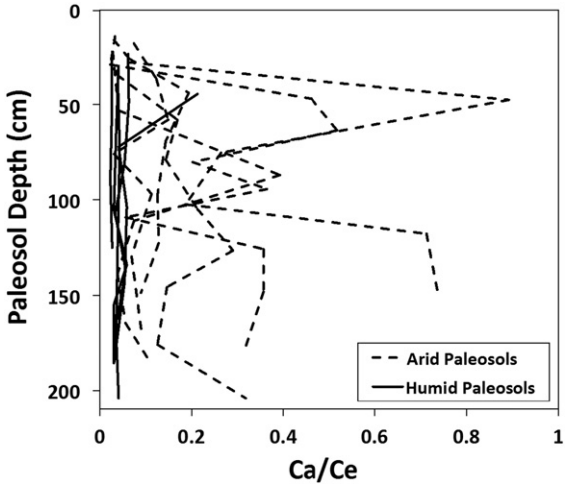

Fig. 5. Comparison of calcium to cerium ratios for arid-type and humid-type paleosols showing leaching loss of calcium relative to the index element cerium in humid-type paleosols, and calcium accumulation relative to cerium in arid-type paleosols.

and there is generally good agreement between the clast coating and fine matrix carbonate in the El Tesoro paleosols (Table 1 and discussed more below).

The source of calcium in pedogenic carbonate is either parent material dissolution or influx of exogenous material from outside the soil system, in this case by eolian deposition of calcium bearing dust. We found that the carbonate bearing paleosols are devoid of carbonate in their upper horizons, but are immediately overlain by carbonate containing sediment. This pattern shows that (1) the profiles were leached of carbonate in their upper horizons before burial, a feature common in deserts such as the Mojave (Quade et al., 1989; Wang et al., 1996), and (2) there was no vertical overprinting from overlying calcareous sediments following burial, and that (3) C and O stable isotope values and depth profiles are consistent with a pedogenic origin for carbonate in the paleosols and not a limestone (marine) source, as discussed more below.

The time interval that each paleosol experienced before burial is not essential to detecting the signal of the climate. However, it can assist in understanding the rate of sedimentation. It is common in arid settings, if carbonate deposition rates are broadly known, to use the inventory of total carbonate (usually derived from atmospheric deposition) as a guide to duration of exposure. The source of calcium, particularly in semi-arid to arid settings where *in situ* weathering is minimal, is eolian deposition of calcium-bearing dust. In the modern Atacama Desert, deposition has been measured to be 3 ± 2 mmol Ca m^{-2} $year^{-1}$, an average of six measurements made at three sites approximately 150 to 500 km south of El Tesoro with a MAP gradient across sites of 2 to 20 mm $year^{-1}$ (Ewing et al., 2006). These deposition rates, while seemingly appropriate for the Quaternary, may not fully represent early Cenozoic conditions, but fall within that found in arid settings (<1–120 mmol Ca m^{-2} $year^{-1}$, Reheis et al., 1995).

Estimates of soil exposure duration times can be calculated from carbonate weight % in the <2 mm fine fraction determined during mass spectrometric analyses for C and O stable isotopes. Carbonate weight % was calculated for the thickness of each carbonate-bearing horizon, and horizons were summed for each calcareous paleosol (Table 1). The total carbonate abundance for each paleosol was divided by the modern eolian Ca dust flux rate of 3 ± 2 mmol Ca m^{-2} $year^{-1}$ (Ewing et al., 2006), yielding an estimated exposure duration age for each calcareous soil. While this simple calculation contains considerable uncertainties, we use these exposure time estimates only to illustrate that the soil-forming environments may have spanned approximately 10 Ma in total, which is similar to the age interval indicated by the underlying Cu mineralization and overlying ignimbrite units (within uncertainty). Later in the Miocene, sedimentation nearby seems to have ceased, and thick hyperarid paleosols developed. Rech et al. (2006) estimated that a 6-m-thick series of calcic and argillic paleosols found in the upper reaches of the Calama Basin approximately 100 km to the northeast of El Tesoro formed between 13 and 8 Ma, over the course of 2–5 million years.

5.4. Paleosol carbonate C and O stable isotopes

Pedogenic carbonate $\delta^{13}C$ values from the 12 carbonate-bearing paleosols range from −5.71‰ to 2.70‰ (VPDB) (Fig. 6; Table 1). While the C isotope composition of the atmosphere at this time is not precisely known, carbonate values ranging from 4‰ to 5‰ (or 8‰ to 9‰ if diffusional effects are added) would reflect entirely abiotic C, and so it is clear that the pedogenic carbonate is indicative of significant plant-derived CO_2. None of the paleosols show the typical increase in C isotope values with decreasing depth (c.f. Cerling, 1984), which may be a result of truncation and removal of shallow paleosol horizons that may have contained carbonate with higher $\delta^{13}C$ values, reflecting the influence of atmospheric CO_2. The depth of carbonate-bearing Bk horizons varied from 25 cm to more than 100 cm (and the absolute loss of overlying A horizons is not well constrained). Thus, it is plausible that all C

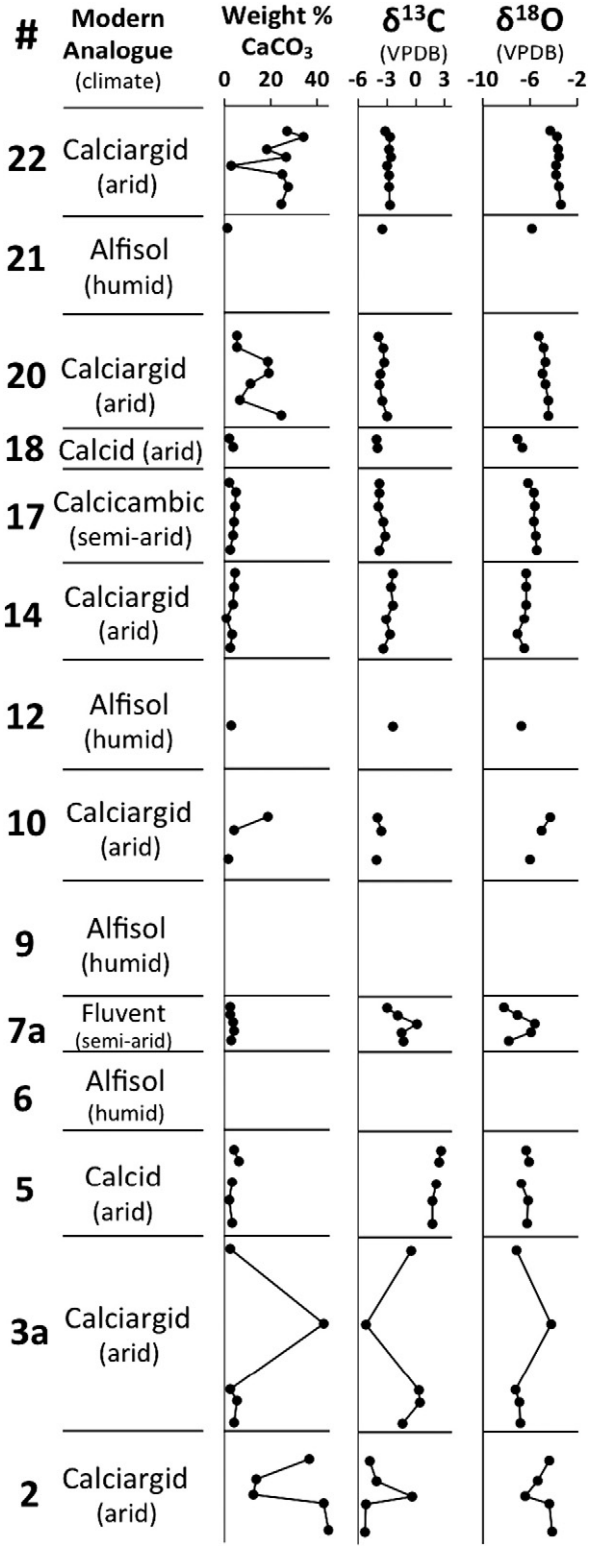

Fig. 6. Simplified stratigraphic arrangement of paleosols at El Tesoro (non-pedogenic gravels in between paleosols not shown for clarity) with analogous modern soils, climate interpretations, and pedogenic carbonate stable isotope values.

isotope depth profiles reflect relatively deep soil conditions and thus reflect depth-invariant paleo-soil CO_2 values that may occur below 50 or more cm from the surface (Cerling, 1984). The range in $\delta^{13}C$ values up section of paleosol 9 suggests soil CO_2 $\delta^{13}C$ values of ca. −17‰ to −19‰ indicating modest rates of soil CO_2 production (Cerling, 1984) in the carbonate-forming environment. Carbonate $\delta^{13}C$ values

of the lower calcareous paleosols (7a, 3a, 2) have higher values and variability, suggestive of periods of lower soil respiration and greater aridity than for soils found higher in the stratigraphic section.

The $\delta^{18}O$ values of carbonate ranged from -8.79‰ to −3.16‰ (VPDB) (Fig. 6; Table 1). None of the paleosol profiles had distinctive depth trends, indicating that the ratio of transpiration/evaporation in terms of soil water loss was relatively high—or that the depth of carbonate formation was below zones of significant evaporative enrichment (e.g. Barnes and Allison, 1983, 1988). Carbonate $\delta^{18}O$ values of the lower calcareous paleosols (7a, 3a, 2) have intra-paleosol variability in their $\delta^{18}O$ values that mirrors the C isotope patterns. $\delta^{18}O$ values in the upper part of the section (14, 17, 20, 22) all shift towards heavier values, trending from an average of −6.28‰ in paleosol 14 to an average of −3.78‰ in 22. This trend in $\delta^{18}O$ values is not reflected in the $\delta^{13}C$ values.

6. Paleoclimate discussion

The most unambiguous indicator of the climatic conditions when the Tesoro sediments were accumulating and undergoing soil formation is the presence or absence of secondary carbonate. The presence of pedogenic carbonate definitively shows that this region of the Atacama Desert was not hyperarid during the early and mid-Miocene because pedogenic carbonate requires a minimum level of precipitation that can support vegetation and create adequate respired CO_2 in order for carbonates to form (Quade et al., 2007). Rech et al. (2006) reported argillic and calcic paleosols of early Miocene age (ca. 20 Ma) approximately 100 km to the northeast of El Tesoro in the Calama Basin. Those paleosols were reported to have montmorillonite and illite clay minerals in their argillic horizons, which are found in soil-forming environments with up to 500 to 1000 mm/year of precipitation (Schaetzel and Anderson, 2005), conditions that are also suggested by the argillic El Tesoro paleosols (#6, 9, 12, and 21). The El Tesoro paleosols show that the climate in the vicinity of Calama has greatly aridified since the more humid periods of the early and mid-Miocene. A regionally wetter climate in northern Chile during the Oligo-Miocene is also supported by the presence of fluvial gravel deposits and relict alluvial fans at latitudes of 19° to 23°S (May et al., 1999; Sáez et al., 1999; Hartley and Evenstar, 2010). The present elevation at which precipitation is high enough to form pedogenic carbonate is now ~3200 masl (Quade et al., 2007). The elevation at which the El Tesoro paleosols originally formed may have been much lower based on estimates of 2840 m (±2510 m) of regional uplift during the early and middle Miocene (Jordan et al., 2010). In the Tarapaca region north of El Tesoro, Farías et al. (2005) determined that pluvial conditions existed at elevations as low as 1200 masl during the early to mid-Miocene.

The C stable isotope composition offers a perspective on changes in ecosystem productivity over time. The C isotope composition is a function of both rates of (i) soil respiration, and (ii) atmospheric CO_2 concentrations. The ratio between the two sources is driven by variations in soil and plant respiration and/or variations in atmospheric CO_2 partial pressures (Cerling, 1991). A mixing model that relates measured pedogenic carbonate $\delta^{13}C$ values to soil CO_2 concentrations can be reformulated from Yapp and Poths (1996) as (Myers et al., 2012):

$$C_S = C_A\left(\left(\delta^{13}C_A - \delta^{13}C_O\right)/\left(\delta^{13}C_C - \delta^{13}C_O\right)\right) \quad (1)$$

where C is the concentration (in ppmV) of CO_2, and $\delta^{13}C_X$ are the $\delta^{13}C$ values of carbonate formed in equilibrium with: soil (S), atmosphere (A), soil organic matter (O), and the measured $\delta^{13}C$ values of pedogenic carbonate (C).

Atmospheric CO_2 concentrations during the Miocene are estimated to be $C_A = 250$ ppm (Pagani et al., 1999), with $\delta^{13}C_A$ value = −6.5‰ (Ekart et al., 1999). A $\delta^{13}C_O$ value of −6.41‰ was used in Eq. (1), which reflects carbonate formed at 25 °C in equilibrium with soil CO_2 having a $\delta^{13}C$ value of −20.6‰, which reflects soil CO_2 derived from C3-type soil organic matter with a $\delta^{13}C$ value of −25‰ (+a 4.4‰ diffusional correction). Soil CO_2 concentrations obtained from Eq. (1) range from 266 ppm to 3464 ppm, using the minimum and maximum paleosol $\delta^{13}C_C$ values of −5.71‰ and 2.70‰ (Table 1).

These estimates of soil CO_2 concentrations at El Tesoro in the early to mid-Miocene are similar to soil CO_2 concentrations measured in modern carbonate-forming soils that receive approximately 100 to 220 mm MAP (Breecker et al., 2009). The $\delta^{13}C$ values of paleosol pedogenic carbonate at El Tesoro also fall within the range of modern soils in Argentina, east of Santiago, Chile that have MAP ranging from 132 to 320 mm $year^{-1}$ (Peters et al., 2013). These comparisons with modern pedogenic carbonate-forming environments provides significant support for Miocene conditions with rainfall values an order of magnitude higher than the present amounts, which is 4.2 mm at nearby Calama (Houston, 2006). It also requires active plant cover and biological CO_2 production, which is presently entirely absent at El Tesoro.

The $\delta^{18}O$ value of pedogenic carbonate is controlled by both (i) the $\delta^{18}O$ value of soil water from which the carbonate formed and (ii) the temperature during carbonate formation (Cerling, 1984). Here, we assume a temperature of 25 °C and no evaporative enrichment of soil water, based on the lack of depth-dependent O isotope profiles in any of the paleosols and the relatively deep carbonate formation zones inferred by evidence of upper soil truncation. Using the relations of Kim and O'Neil (1997), the $\delta^{18}O$ values of the soil water that the carbonates formed from ranges from −0.45‰ to −12.03‰, with a mean of −2.92‰ (VSMOW). The range in $\delta^{18}O$ values of the El Tesoro paleosols encompasses that observed in modern soils in Argentina at elevations of 1000 to 2000 masl (Peters et al., 2013). The $\delta^{18}O$ value of present rainwater in the area and at similar elevations to modern El Tesoro is approximately −5‰ (Aravena et al., 1999; Rech et al., 2010).

Globally, the early and mid-Miocene were dynamic times climatically as the Earth system cooled from the warm conditions of the early Eocene climatic optimum (Zachos et al., 2001). The Antarctic ice sheet is thought to have started to form during the Oligocene, and by the early Miocene it may have been well developed and extensive (Zachos and Kump, 2005). From a tectonic perspective, the South American continent was fairly close to its present position (Hartley et al., 2005). The Humboldt Current along the western margin of South America was active in this time period after being established in the early Cenozoic (Keller et al., 1997). Various geodynamic scenarios for the Andean Orogeny have been proposed and can be generally framed into two end members: a slow and steady rise beginning as early as the Eocene that results in central Andean elevations of ~2 km during the Miocene (Barnes and Ehlers, 2009), and a rapid rise model that purports a major uplift during the late Miocene resulting in the attainment of current Andean elevations (Garzione et al., 2008).

Oxygen isotopes in paleosol carbonates are widely used in mountain environments as a proxy for paleo-elevation and temperature. It is assumed in these studies that the $\delta^{18}O$ value of rainfall follows a simple relationship with elevation: as elevation increases, temperatures cool, and precipitation $\delta^{18}O$ values decline (cf. Blisniuk and Stern, 2005). This strategy has been used in several studies of paleosols and freshwater carbonates on both the eastern and western margins of the Andes in northern Chile and Bolivia (Garzione et al., 2006; Quade et al., 2007; Garzione et al., 2008; Rech et al., 2010). Here, we compile these previous results, and include the El Tesoro carbonates for comparison.

In the early Miocene, it appears that both the east and western margins of the present Andean plateau had similar $\delta^{18}O$ values, with the western margin (both El Tesoro and data of Rech et al., 2010) being slightly more positive (Fig. 7). The data also show a sharp divergence of O isotope values over time beginning ca. 20 Ma, with pedogenic carbonate samples from the east on the Altiplano becoming more negative, and the western slope (around El Tesoro and Calama) becoming more positive. The trends shown in Fig. 7 for the Altiplano samples have been used to support the interpretation of significant late Miocene uplift

of the Altiplano (Garzione et al., 2006, 2008). The trend of increasing $\delta^{18}O$ values with decreasing age for the Calama region conflicts with a simple elevation / $\delta^{18}O$ relationship, especially in light of independent observations of uplift (Rech et al., 2006; Jordan et al., 2010). Rech et al. (2010) interpreted their O isotope data to reflect meteoric water that both decreased due to increasing elevation to the east, combined with increasing evaporation in the soil environment, resulting in a net increase in soil carbonate $\delta^{18}O$ values over time. An alternative explanation has recently been proposed by Poulsen et al. (2010), who used regional climate model simulations with variable topographic scenarios. These authors show that uplift of the Andes may produce complex changes in regional circulation and resulting precipitation $\delta^{18}O$ values during the rise of the Andean plateau. From their simulations, precipitation on the Andean Plateau may have experienced *higher* precipitation $\delta^{18}O$ values as the Andes reached mid-elevations due to the onset of convective storms, and increased precipitation rates that enhanced the isotope amount effect. Subsequently, as the Andes rose further, $\delta^{18}O$ values declined due to adiabatic cooling and colder vapor condensation temperatures. Thus, the existing O isotope record (Fig. 7) may be alternatively interpreted as faithfully recording the O isotope composition of regional precipitation as this section of South America underwent both topographic and climatic reorganization over time. Regardless of the mechanism, there is a clear meteoric water disconnection between the eastern and western Andes over the late Cenozoic, one that likely has its origin in complex circulation changes associated with this topographic change.

7. Conclusions

The El Tesoro paleosols represent a remarkable period of oscillations between relatively moist to semi-arid and arid climates during the mid-Cenozoic, in what is now the driest part of the world. The paleosols, combined with other published studies, indicates that this region underwent significant aridification in the late Miocene or later. The O isotope data from these paleosols, when combined with published data from the region, reveal a significant divergence of the O isotope composition of precipitation in the east and western margins of the Andean plateau since 21.9 Ma, and suggest that simple assumptions of decreases in $\delta^{18}O$ values of carbonate with increasing elevation may not apply where topographic change may induce regional circulation changes. However, this also suggests that there may be a richer record of climate embedded in pedogenic carbonate, one that will further our understanding of the rise of the Andes.

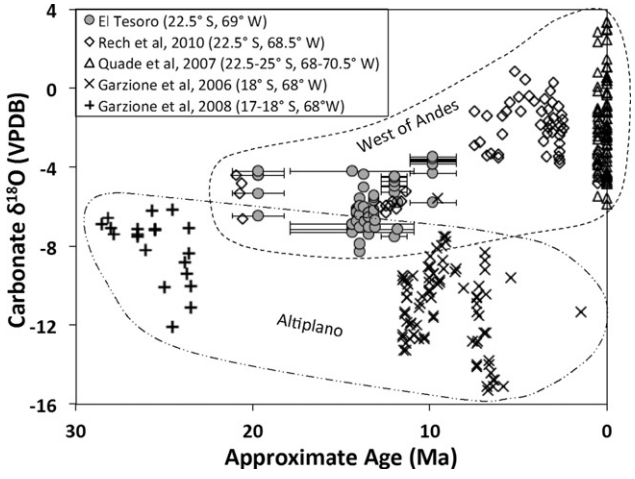

Fig. 7. Comparison of El Tesoro pedogenic carbonate $\delta^{18}O$ values with regional published O isotope data for modern soils, paleosols, and lacustrine and palustrine carbonates on the western side of the Andes near Calama (Quade et al., 2007; Rech et al., 2010) and on the Altiplano (Garzione et al., 2006, 2008). El Tesoro paleosol carbonate ages are estimated from carbonate accumulation times summed over each paleosol and plotted here based on aggradation and soil formation subsequent to Cu mineralization at 21.9 Ma. Error bars on El Tesoro paleosol ages are based on modern carbonate dust flux rate uncertainties (see Section 5.3 and Table 1).

Acknowledgements

We gratefully acknowledge the mine access, support, and survey work of Compania Minera El Tesoro, support from NSF Geobiology and Low Temperature Geochemistry program, and the University of California Agricultural Experiment Station. This paper was improved by the editorial input of Thierry Correge and the reviews of Martin Reich, Adrian Hartley and an anonymous reviewer.

Appendix A. Supplementary data

Supplementary data to this article can be found online at http://dx.doi.org/10.1016/j.palaeo.2015.10.038.

References

Alpers, C., Brimhall, G., 1988. Middle Miocene climatic change in the Atacama Desert, northern Chile: evidence from supergene mineralization at La Escondida. Geol. Soc. Am. Bull. 100, 1640–1656.
Amundson, R., Graham, R.C., Franco-Vizcaino, E., 1997. Orientation of carbonate laminations in gravely soils along a winter/summer precipitation gradient in Baja California, Mexico. Soil Sci. 162 (12), 940–952.
Amundson, R., Dietrich, W., Bellugi, D., Ewing, S., Nishiizumi, K., Chong, G., Owen, J., Finkel, R., Heimsath, A., Stewart, B., Caffee, M., 2012. Geomorphologic evidence for the late Pliocene onset of hyperaridity in the Atacama Desert. Geol. Soc. Am. Bull. 124 (7–8), 1048–1070.
Aravena, R., Suzuki, O., Pena, H., Pollastri, A., Fuenzalida, H., Grilli, A., 1999. Isotopic composition and origin of the precipitation in Northern Chile. Appl. Geochem. 14 (4), 411–422.
Barnes, C.J., Allison, G.B., 1983. The distribution of deuterium and ^{18}O in dry soils: 1. Theory. J. Hydrol. 60 (1), 141–156.
Barnes, C.J., Allison, G.B., 1988. Tracing of water movement in the unsaturated zone using stable isotopes of hydrogen and oxygen. J. Hydrol. 100 (1), 143–176.
Barnes, J.B., Ehlers, T.A., 2009. End member models for Andean Plateau uplift. Earth-Sci. Rev. 97, 117–144.
Blisniuk, P.M., Stern, L.A., 2005. Stable isotope paleoaltimetry: a critical review. Am. J. Sci. 305 (10), 1033–1074.
Breecker, D.O., Sharp, Z.D., McFadden, L.D., 2009. Seasonal bias in the formation and stable isotopic composition of pedogenic carbonate in modem soils from central New Mexico, USA. Geol. Soc. Am. Bull. 121 (3–4), 630–640.
Brimhall, G., Dietrich, W., 1987. Constitutive mass balance relations between chemical composition, volume, density, porosity, and strain in metasomatic hydrochemical systems: results on weathering and pedogenesis. Geochim. Cosmochim. Acta 51, 567–587.
Cerling, T.E., 1984. The stable isotopic composition of modern soil carbonate and its relationship to climate. Earth Planet. Sci. Lett. 71 (2), 229–240.
Cerling, T.E., 1991. Carbon-dioxide in the atmosphere—evidence from Cenozoic and Mesozoic paleosols. Am. J. Sci. 291 (4), 377–400.
Clarke, J.D.A., 2006. Antiquity of aridity in the Chilean Atacama Desert. Geomorphology 73, 101–114.
Coplen, T.B., 1994. Reporting of stable hydrogen, carbon, and oxygen isotopic abundances (technical report). Pure Appl. Chem. 66 (2), 273–276.
De Silva, S., 1989. Geochronology and stratigraphy of the ignimbrites from the 21 30′ S to 23 30′ S portion of the Central Andes of northern Chile. J. Volcanol. Geotherm. Res. 37 (2), 93–131.
Dunai, T.J., González López, G.A., Juez-Larré, J., 2005. Oligocene–Miocene age of aridity in the Atacama Desert revealed by exposure dating of erosion-sensitive landforms. Geology 33 (4), 321.
Ekart, D.D., Cerling, T.E., Montanez, I.P., Tabor, N.J., 1999. A 400 million year carbon isotope record of pedogenic carbonate: implications for paleoatmospheric carbon dioxide. Am. J. Sci. 299 (10), 805–827.
Evenstar, L.A., Hartley, A.J., Stuart, F.M., Mather, A.E., Rice, C.M., Chong, G., 2009. Multiphase development of the Atacama planation surface recorded by cosmogenic 3He exposure ages: implications for uplift and Cenozoic climate change in western South America. Geology 37 (1), 27–30.
Ewing, S., Sutter, B., Owen, J., Nishiizumi, K., Sharp, W., Cliff, S., Perry, K., Dietrich, W., McKay, C., Amundson, R., 2006. A threshold in soil formation at Earth's arid–hyperarid transition. Geochim. Cosmochim. Acta 70 (21), 5293–5322.
Farías, M., Charrier, R., Comte, D., Martinod, J., Hérail, G., 2005. Late Cenozoic deformation and uplift of the western flank of the Altiplano: evidence from the depositional, tectonic, and geomorphologic evolution and shallow seismic activity (northern Chile at 19 30′ S). Tectonics 24 (4).
Garzione, C.N., Molnar, P., Libarkin, J.C., MacFadden, B.J., 2006. Rapid late Miocene rise of the Bolivian Altiplano: evidence for removal of mantle lithosphere. Earth Planet. Sci. Lett. 241 (3–4), 543–556.

Garzione, C.N., Hoke, G.D., Libarkin, J.C., Withers, S., MacFadden, B., Eiler, J., Ghosh, P., Mulch, A., 2008. Rise of the Andes. Science 320 (5881), 1304–1307.
Gile, L.H., Peterson, F.F., Grossman, R.B., 1966. Morphological and genetic sequences of carbonate accumulation in desert soils. Soil Sci. 101 (5), 347–360.
Gromet, L.P., Silver, L.T., 1983. Rare earth element distributions among minerals in a granodiorite and their petrogenetic implications. Geochim. Cosmochim. Acta 47, 925–939.
Hartley, A.J., Chong, G., 2002. Late Pliocene age for the Atacama Desert: implications for the desertification of western South America. Geology 30 (1), 43.
Hartley, A.J., Evenstar, L., 2010. Cenozoic stratigraphic development in the north Chilean forearc: implications for basin development and uplift history of the Central Andean margin. Tectonophysics 495 (1), 67–77.
Hartley, A.J., Chong, G., Houston, J., Mather, A.E., 2005. 150 million years of climatic stability: evidence from the Atacama Desert, northern Chile. J. Geol. Soc. 162 (3), 421–424.
Houston, J., 2006. Variability of precipitation in the Atacama Desert: its causes and hydrological impact. Int. J. Climatol. 26 (15), 2181–2198.
Jordan, T.E., Nester, P.L., Blanco, N., Hoke, G.D., Dávila, F., Tomlinson, A.J., 2010. Uplift of the Altiplano-Puna plateau: a view from the west. Tectonics 29 (5), TC5007.
Jordan, T.E., Kirk-Lawlor, N.E., Blanco, N.P., Rech, J.A., Cosentino, N.J., 2014. Landscape modification in response to repeated onset of hyperarid paleoclimate states since 14 Ma, Atacama Desert, Chile. Geol. Soc. Am. Bull. 126 (7–8), 1016–1046.
Keller, G., Adatte, T., Hollis, C., Ordonez, M., Zambrabo, I., Jimenez, N., Stinnesbeck, W., Aleman, A., Hale-Erlich, W., 1997. The Cretaceous/Tertiary boundary event in Ecuador: reduced biotic effects due to eastern boundary current setting. Mar. Micropaleontol. 31, 97–133.
Kim, S.T., O'Neil, J.R., 1997. Equilibrium and nonequilibrium oxygen isotope effects in synthetic carbonates. Geochim. Cosmochim. Acta 61 (16), 3461–3475.
Kurtz, A.C., Derry, L.A., Chadwick, O.A., Alfano, M.J., 2000. Refractory element mobility in volcanic soils. Geology 28 (8), 683–686.
Mack, G.H., James, W.C., Monger, H.C., 1993. Classification of paleosols. Geol. Soc. Am. Bull. 105 (2), 129–136.
May, G., Hartley, A., Stuart, F., Chong, G., 1999. Tectonic signatures in arid continental basins: an example from the Upper Miocene–Pleistocene, Calama Basin, Andean forearc, northern Chile. Palaeogeogr. Palaeoclimatol. Palaeoecol. 151 (1), 55–77.
Mora, R., Artal, J., Brockway, H., Martinez, E., Muhr, R., 2004. El Tesoro exotic copper deposit, Antofagasta Region, Northern Chile. Society of Economic Geologists, Special Publication no. 11 pp. 187–197.
Myers, T.S., Tabor, N.J., Jacobs, L.L., Mateus, O., 2012. Estimating soil pCO_2 using paleosol carbonates: implications for the relationship between primary productivity and faunal richness in ancient terrestrial ecosystems. Paleobiology 38 (4), 585–604.
Pagani, M., Arthur, M.A., Freeman, K.H., 1999. Miocene evolution of atmospheric carbon dioxide. Paleoceanography 14 (3), 273–292.
Peters, N.A., Huntington, K.W., Hoke, G.D., 2013. Hot or not? Impact of seasonally variable soil carbonate formation on paleotemperature and O-isotope records from clumped isotope thermometry. Earth Planet. Sci. Lett. 361, 208–218.
Poulsen, C.J., Ehlers, T.A., Insel, N., 2010. Onset of convective rainfall during gradual Late Miocene rise of the Central Andes. Science 328, 490–493.
Quade, J., Cerling, T.E., Bowman, J.R., 1989. Systematic variations in the carbon and oxygen isotopic composition of pedogenic carbonate along elevation transects in the southern Great Basin, United States. Geol. Soc. Am. Bull. 101 (4), 464–475.
Quade, J., Rech, J.A., Latorre, C., Betancourt, J.L., Gleeson, E., Kalin, M.T.K., 2007. Soils at the hyperarid margin: the isotopic composition of soil carbonate from the Atacama Desert, Northern Chile. Geochim. Cosmochim. Acta 71, 3772–3795.
Rech, J.A., Currie, B.S., Michalski, G., Cowan, A.M., 2006. Neogene climate change and uplift in the Atacama Desert, Chile. Geology 34 (9), 761–764.
Rech, J.A., Currie, B.S., Shullenberger, E.D., Dunagan, S.P., Jordan, T.E., Blanco, N., Tomlinson, A.J., Rowe, H.D., Houston, J., 2010. Evidence for the development of the Andean rain shadow from a Neogene isotopic record in the Atacama Desert, Chile. Earth Planet. Sci. Lett. 292, 371–382.
Reheis, M.C., Goodmacher, J.C., Harden, J.W., McFadden, L.D., Rockwell, T.K., Shroba, R.R., Taylor, E.M., 1995. Quaternary soils and dust deposition in southern Nevada and California. Geol. Soc. Am. Bull. 107 (9), 1003–1022.
Renne, P.R., Balco, G., Ludwig, K.R., Mundil, R., Min, K., 2011. Response to the comment by W.H. Schwarz et al. on "Joint determination of ^{40}K decay constants and $^{40}Ar^*/^{40}K$ for the Fish Canyon sanidine standard, and improved accuracy for $^{40}Ar/^{39}Ar$ geochronology" by P.R. Renne et al. (2010). Geochim. Cosmochim. Acta 75, 5097–5100.
Sáez, A., Cabrera, L., Jensen, A., Chong, G., 1999. Late Neogene lacustrine record and palaeogeography in the Quillagua–Llamara basin, Central Andean fore-arc (northern Chile). Palaeogeogr. Palaeoclimatol. Palaeoecol. 151 (1), 5–37.
Schaetzel, R., Anderson, S., 2005. Soils: Genesis and Geomorphology. Cambridge University Press, New York (817 pp.).
Sernageomin, 2011. Informe de datacion radiometrica K-Ar Numero 32/2011. Servicio Nacional de Geologia y Minera, Subdireccion Nacionalde Geologia, Departmento de Laboratorios, Chile.
Soil Survey Staff, 1999. Soil taxonomy: a basic system of soil classification for making and interpreting soil surveys. Natural Resources Conservation Service, United States Department of Agriculture.
Suarez, M., Bell, C., 1987. Upper Triassic to Lower Cretaceous continental and coastal saline lake evaporites in the Atacama region of northern Chile. Geol. Mag. 124 (5), 467–475.
Tapia, M., Riquelme, R., Campos, E., Marquardt, C., Mpodozis, C., Mora, R., Munchmeyer, C., 2011. Cenozoic exotic Cu mineralization in the Centinela District (Atacama Desert, Northern Chile). Society for Geology Applied to Mineral Deposits, 11th Biennial Meeting: Antofagasta. Chile.
Wang, Y., McDonald, E., Amundson, R., McFadden, L., Chadwick, O., 1996. An isotopic study of soils in chronological sequences of alluvial deposits, Providence Mountains, California. Geol. Soc. Am. Bull. 108 (4), 379–391.
Yapp, C.J., Poths, H., 1996. Carbon isotopes in continental weathering environments and variations in ancient atmospheric CO_2 pressure. Earth Planet. Sci. Lett. 137 (1), 71–82.
Zachos, J.C., Kump, L., 2005. Carbon cycle feedbacks and the initiation of Antarctic glaciation during the earliest Oligocene. Glob. Planet. Chang. 47, 51–66.
Zachos, J., Pagani, M., Sloan, L., Thomas, E., Billups, K., 2001. Trends, rhythms, and aberrations in global climate 65 Ma to present. Science 292 (5517), 686–693.